ELSEVIER

Journal of Nuclear Materials 266–269 (1999) 75–83

journal of nuclear materials

Plasma wall interaction and plasma edge properties with radiation cooling and improved confinement in TEXTOR-94

B. Unterberg [a,*], M. Brix [a], R. Jaspers [b], A. Kreter [a], Y.M. Kim [a], M. Lehnen [a], Ph. Mertens [a], A.M. Messiaen [c], J. Ongena [c], V. Philipps [a], A. Pospieszczyk [a], U. Samm [a], B. Schweer [a]

[a] *Institut für Plasmaphysik* [1], *Forschungszentrum Jülich GmbH, EURATOM-Association, D-52425 Jülich, Germany*
[b] *FOM-Instituut voor Plasmafysica*[1], *Rijnhuizen, EURATOM-Association, Nieuwegein, The Netherlands*
[c] *Laboratoire de Physique de Plasmas/Laboratorium voor Plasmafysica*[1], *Ecole Royale Militaire/Koninklijke Militaire School, EURATOM-Association, B-1000 Brussels, Belgium*

Abstract

The Radiative Improved Mode obtained on the limiter tokamak TEXTOR-94 combines power exhaust by a radiating plasma boundary with improved energy confinement (as good as in the ELM-free H-mode in divertor tokamaks) at high plasma densities (equal to or even above the Greenwald density) in quasi-stationary discharges. Substantial changes of the plasma edge properties are observed with increasing radiation: a reduction of the plasma edge density and temperature, a reduction of particle transport out of the confined plasma volume and an increase of the penetration depth and of the fueling efficiency of neutrals. In addition to an increased inward drift this causes a steepening of the density profiles. For a given plasma current and heating scenario the transition to improved confinement takes place as soon as the density peaking reaches a critical threshold. With the injection of neon an increased sputtering yield of carbon and in addition photon induced desorption of oxygen from the wall are observed, leading to an increased dilution at the plasma edge, whereas the central dilution is only weakly affected.

Keywords: Radiative layer; Enhanced confinement; Edge plasma; Impurity release; TEXTOR

1. Introduction

Power exhaust is one of the outstanding problems on the way to a burning fusion plasma. The *concept of a cold, radiating plasma mantle* is considered as a possible solution of this problem: line radiation by impurities distributes the power over large areas, thereby avoiding unacceptably high localized heat loads to the plasma facing components. However, at the same time many other important requirements have to be met: good energy confinement, high density operation, efficient helium exhaust, sufficiently low impurity concentration in the fusion volume as well as stationarity of the plasma.

First experiments at the tokamak TEXTOR showed the feasibility of the such a concept under quasi-stationary conditions in auxiliary heated discharges using neon and/or silicon as radiating species [1,2]. Contrary to the common belief, a high radiation level can lead to a substantial improvement of the energy confinement under appropriate heating and operational scenarios. This regime, the Radiative Improved-Mode (RI-mode), is characterized by the following features: *good energy confinement* (as good as in ELM- free H-mode discharges in divertor machines), *high density operation* (around the empirical Greenwald density n_{GW} [3]) and *heat exhaust by impurity radiation* at the plasma boundary *under quasi-stationary conditions* (duration of the quasi-stationary phase up to 100 confinement times)

* Corresponding author. Tel.: +49 2461 61 4803; fax: +49 2461 61 5452; e-mail: B.Unterberg@fz-juelich.de

[1] Affiliations a, b and c are partners in the Trilateral Euregio Cluster.

0022-3115/99/$ – see front matter
PII: S0022-3115(98)00821-6

[4,5]. In contrast to H-mode discharges in divertor tokamaks, there is no degradation of confinement when going to higher density but a favorable *linear increase of the energy confinement time with density* is observed [6,7]. Improved energy confinement in discharges with a radiating boundary has also been found in divertor machines like ASDEX-upgrade (CDH-mode [8] and improved L-mode [9]) and on DIII-D [10,11].

There is a twofold importance of the plasma edge in the RI-mode at TEXTOR-94: on one hand, the changes of plasma edge parameters (i.e. reduction of the edge temperature and of the convective heat flux to the limiters) are the primary intention of the radiation cooling, on the other hand, these changes are an essential ingredient to obtain improved confinement. It turns out that the changes of the global recycling and fueling properties associated with the reduction of plasma edge temperature and density with increasing radiation are of major importance for the confinement quality. The aim of this paper is to describe the variation of plasma edge characteristics when a radiating boundary is formed, and to figure out the link between the plasma edge and the global confinement properties of the RI-mode.

A critical issue of the concept of radiation cooling is the content of the intrinsic and additionally seeded impurities in the plasma bulk. In this paper the impurity production at the limiters and at the wall is investigated in discharges with a radiating boundary. The resulting dilution of plasma edge and center will be described.

2. Experimental set-up and operational conditions for the RI-mode

TEXTOR-94 is a medium size tokamak ($R = 1.75$ m, $a = 0.46$ m) with a circular cross section equipped with the toroidal pump limiter ALT-II covered by graphite tiles. The RI-mode can be achieved in a wide range of operational parameters with plasma currents from $I_p = 290$ to 500 kA and toroidal magnetic fields from $B_T = 1.7$ to 2.6 T ($q_a = 2.6$–4.7). Deuterium discharges are additionally heated by deuterium neutral beam co-injection (NBI co) alone or in combination with ion cyclotron resonance heating (ICRH) and/or neutral beam counter injection (NBI counter). The RI-mode can be obtained with fully balanced neutral beam injection. Nevertheless, a minimum fraction of about 20% of the input power by neutral beam co-injection is found to be necessary to establish RI-mode conditions. The radiation cooling is established by feedback controlled injection of neon or argon. Wall coating by plasma assisted deposition of silicon (siliconization [12]) and the subsequent release of silicon from the plasma facing components by sputtering is also suited to establish a radiating boundary and improved energy confinement.

In this paper we focus on discharges with a plasma current of $I_p = 400$ kA and a toroidal field of $B_T = 2.25$ T ($q_a = 3.2$) heated with NBI co and ICRH under boronized conditions. Neon is used to establish the radiating boundary.

Beside the standard diagnostics for the plasma bulk a wide selection of edge diagnostics are used to determine the physical quantities of interest: To determine the deuterium, the carbon and oxygen fluxes at the main ALT-II limiter emission spectroscopy of D_α ($\lambda = 656.1$ nm), CI ($\lambda = 909.5$ nm) and OI ($\lambda = 844.6$ nm) has been used [13]. The variation of the conversion factors S/XB (S: ionization rate coefficient, X: excitation rate coefficient and B branching ratio of the transition observed) between measured intensity and resulting flux with the electron temperature at the limiter has been taken into account. We have corrected the conversion factor for D_α to take into account the molecular contribution to the recycling flux, which is of the same magnitude as the atomic flux for the high density conditions considered in this paper. As a substantial part of the molecules dissociates into ions, S/XB has to be increased (s. discussion in Ref. [14] concerning the role of hydrogen molecules for the determination of recycling fluxes). For the discharges discussed in this paper a value of S/XB (D_α) = 23 has been used. The ion fluxes of deuterium and neon in the SOL have been measured by the Sniffer probe mass spectrometer [15] located at a radius of $R - R_0 = 0.49$ m. The neutral pressure of various species has been determined using a conventional mass spectrometer positioned in the horizontal midplane at the low field side. A thermal He-beam diagnostic with a recalibrated observation system was used to determine the radial electron density and temperature profiles in the plasma edge in the horizontal midplane at the low field side. The evaluation of the data has been performed using a refined collisional–radiative model for the helium atoms [16].

3. The effect of radiation cooling on the plasma edge parameters

Substantial changes of the plasma edge parameters can be observed when the fraction of the radiated power with respect to the total heating power (radiation level γ) is increased using additional impurity seeding. Fig. 1 shows the global discharge parameters for a RI-mode discharge with neon injection at a plasma current of $I_p = 400$ kA (solid lines) in comparison to a L-mode discharge without neon (broken lines). The phase of additional heating with NBI co and ICRH lasts from 1.2 to 5.0 s. Between $t = 1.5$ and $t = 3.8$ s feedback controlled *neon* seeding is applied, leading to a constant γ of 75%. With the increase of γ, a decrease of the electron temperature T_e from 110 down to 65 eV as well

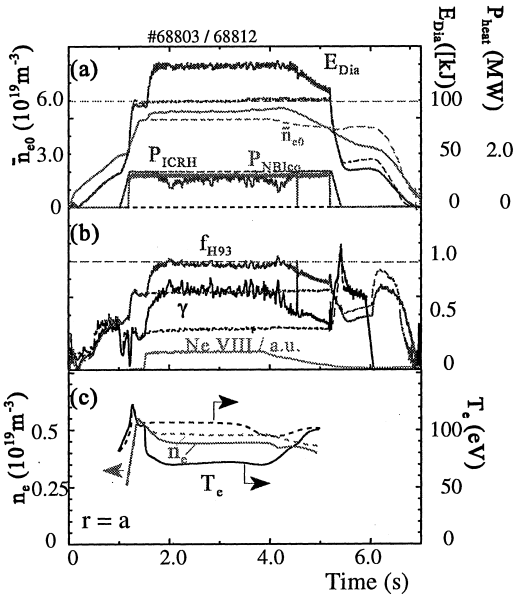

Fig. 1. Typical example of a discharge in the RI-mode with neon injection (solid lines). (a) Diamagnetic energy E_{DIA}, auxiliary heating power of the neutral beam, P_{NBI}, and of the radiofrequency heating, P_{ICHR}, line averaged central electron density $\bar{n}_{e0}$, (b) enhancement factor f_{H93} with respect to the ELM-free H-mode scaling ITERH93-P, radiation level γ, line intensity of the feedback controlled NeVIII, (c) electron density and temperature at the LCFS. The broken curves correspond to a reference discharge in the L-mode without neon seeding.

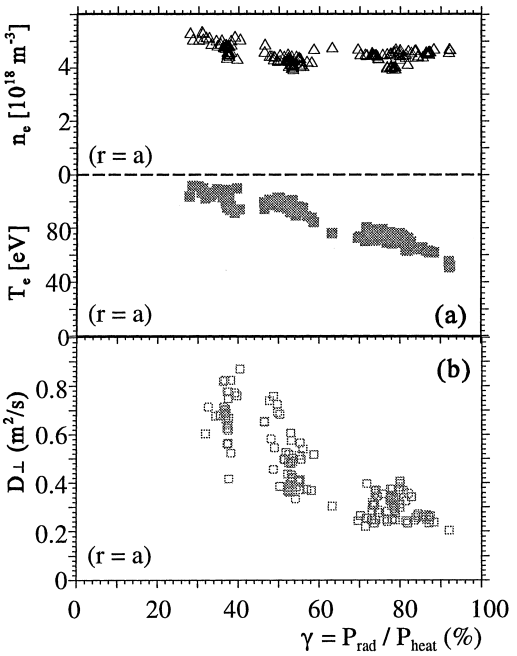

Fig. 2. (a) Electron density n_e and temperature T_e at the LCFS, (b) diffusion coefficient $D_\perp$ at the LCFS against radiation level γ ($\bar{n}_{e0} = 0.9$–$1.0 \times n_{GW}, P_{heat} = 2.2$–$2.7$ MW, $I_p = 400$ kA).

as a slight reduction of the electron density n_e at the LCFS can be observed. When the radiation level γ reaches about 50%, a remarkable increase of the diamagnetic energy up to a preset value of 125 kJ is seen, leading to a slight adjustment of the ICRH-power as a consequence of a feedback on the plasma energy. The improvement of energy confinement is characterized in terms of the ELM-free H-mode scaling [17], leading to an enhancement factor f_{H93} of 0.95. In addition to the improved energy confinement and to the high value of γ, the line averaged central electron density $\bar{n}_{e0}$ reaches a constant value of 90% of the Greenwald density (n_{GW} (10^{20} m^{-3}) = I_P(mA)/(πa(m)^2) = 0.6 for this discharge). In the reference discharge without neon injection the resulting diamagnetic energy remains at 100 kJ ($f_{H93} = 0.7$).

The variation of T_e and n_e at the LCFS with γ for a series of discharges is depicted in Fig. 2(a). From γ = 35% to 90% T_e is reduced by roughly a factor of 2 while n_e decreases slightly by about 15%. The ion temperature T_i (determined by charge exchange measurements of CVI at $\lambda = 529.06$ nm) is found to be about a factor of 1.5–2.0 larger than T_e. The ratio between T_i and T_e does not change significantly with γ. The decay length of the electron density λ_n in the scrape-off layer (SOL) is slightly decreasing with γ from about 12 down to 9 mm whereas the decay length of the electron temperature rises from 25 to 30 mm. Using the electron and ion temperatures measured to calculate the ion sound velocity c_s and the density decay length we estimate the diffusion coefficient at the LCFS according to the simple relation $D_\perp = \lambda_n^2\, c_s/2L_\parallel$ [18]. Here, $L_\parallel$ denotes the connection length in the SOL (for TEXTOR-94 $L_\parallel = 18.6$ m at $I_p = 400$ kA/$B_T = 2.25$ T). The diffusion coefficient decreases from $D_\perp = 0.5$–0.7 m^2 s^{-1} at γ = 35% to $D_\perp = 0.25$ m^2 s^{-1} at γ = 85%, cf. Fig. 2(b). The scatter of the data may be attributed to different fractions of ionization in the SOL for a given γ not taken into account in our calculation. The reduction of the diffusion coefficient with increasing radiation is approximately Bohm-like ($D_\perp \approx 0.2$ D_{Bohm}). Therefore, radiation cooling leads to a substantial *decrease of particle flux out of the confined volume*.

Fig. 3 summarizes the variation of edge density vs. edge temperature at the LCFS in an edge operational diagram. Different symbols indicate the energy confinement time with respect to the ELM-free H-mode using the enhancement factor f_{H93}. In this diagram discharges in the RI-mode (squares, with $f_{H93} > 0.85$, i.e. confinement at least as good as ELMy H-mode) are clearly separated from L-mode discharges (triangles). The boundary can be fairly well described by the relation $n_e\sqrt{T_e} = \text{const}$. This expression can be interpreted as a

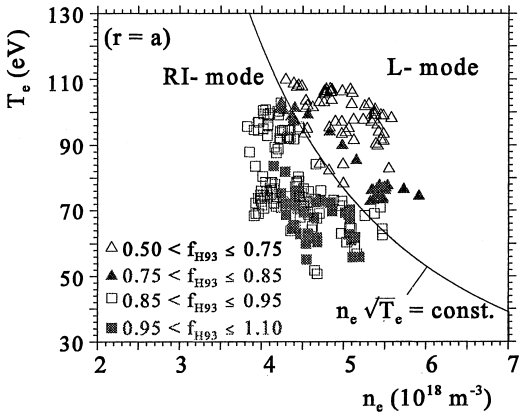

Fig. 3. Edge operational diagram of the RI-mode, different symbols indicate the energy confinement time with respect to the ELM-free H-mode ($\bar{n}_{e0} = 0.8$–$1.1 \times n_{GW}$, $P_{heat} = 2.0$–3.0 MW, $I_p = 400$ kA).

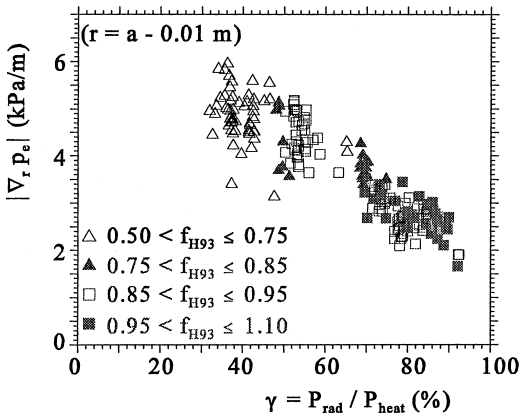

Fig. 4. Radial gradient of the electron pressure at $r = a - 0.01$ against radiation level γ, different symbols indicate energy confinement time with respect to the ELM-free H-mode ($\bar{n}_{e0} = 0.8$–$1.1 \times n_{GW}$, $P_{heat} = 2.0$–3.0 MW, $I_p = 400$ kA).

measure for the ionization rate of neutrals at the LCFS. $\langle\sigma v\rangle_{ion} \sim \sqrt{T_e}$ for D_0 in the temperature range under consideration). It is less a measure of the deuterium flux to the limiter due to different degrees of dilution (cf. discussion in Section 5.) The discharges on the left side of the boundary showing the improved confinement in the RI-mode are therefore characterized by a larger penetration depth of neutrals $\lambda_{i0} = \langle v\rangle_0/(\langle\sigma v\rangle_{ion} n_e)$ for a given neutral velocity $\langle v\rangle_0$ in comparison to the L-mode discharges. These findings clearly show the important role of the neutral fueling which will be discussed more in detail in the next section.

In contrast to what is observed in divertor tokamaks under H-mode conditions (cf. e.g. [19]) there is no formation of an edge pedestal linked to the transition to improved confinement in the RI-mode. On the contrary, the temperature and pressure profiles flatten in the boundary region which is affected by the radiation losses. Fig. 4 shows the radial pressure gradients of electrons 1 cm inside the LCFS. The different symbols depict the energy confinement time with respect to the ELM-free H-mode scaling which is increasing with decreasing pressure gradient. This behavior is clearly different to what is found for H-mode conditions in divertor tokamaks where the global energy confinement is strongly depending on a steepening of the pressure gradient at the edge. However, deviations from the correlation between edge pedestal and stored energy are also found on ASDEX-upgrade for discharges with a radiating boundary in the CDH-mode [20]. The *improved confinement in the RI-mode is not caused by a transport barrier at the edge*. Instead a zone of *reduced transport* is observed *further inside the confined volume*, starting at the minor radius where the radiative mantle ends ($r/a \approx 0.6$) [21].

4. Recycling and fueling characteristics of the RI-mode

The most remarkable change with increasing radiation level γ is the strong reduction of the deuterium flux recycling at the main limiter ALT-II corresponding to the reduction of $D_\perp$ described in the previous section. Fig. 5 shows the total number of deuterons and the total recycling flux for the RI-mode discharge (solid lines) and the reference discharge without neon seeding in the L-mode (broken lines) already described in Fig. 1. The deuteron content has been determined using the total number of electrons measured with the HCN interferometer and correcting for the dilution by impurities using charge exchange measurements of the impurity concentrations of neon, carbon and oxygen in the

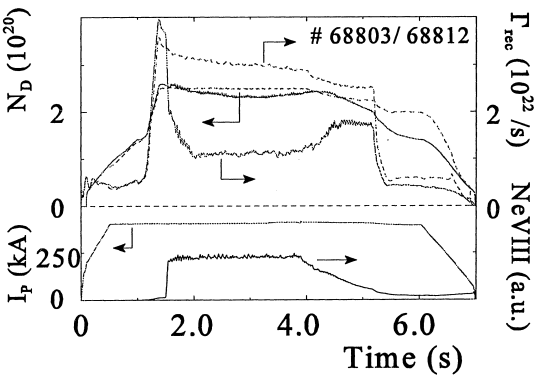

Fig. 5. Time traces of the total recycling flux and the total number of deuterons for a RI-mode discharge (solid lines) and a reference discharge in the L-mode without neon injection (broken lines). The interval of the neon feedback and the flat top phase of the plasma current are indicated by the respective times traces.

plasma bulk (cf. Section 5 for details). To estimate the total recycling flux Γ_{rec} we used the flux measured spectroscopically at the ALT-II limiter taking into account the increase of the S/XB factors by molecules as described in Section 2. The total recycling flux consists of the recycling flux at the limiter and additional flux from the wall estimated to be roughly 30% of the limiter flux independent of γ. Such a percentage can be inferred using an observation of the poloidal cross section of the plasma with a CCD-camera equipped with a D_α interference filter [22]. The assumption of a constant fraction of flux from the wall is motivated by the observation, that the neutral pressure of deuterium measured at the wall in the horizontal mid-plane varies proportional to the flux at ALT-II when changing γ (cf. Figs. 9 and 10). The reduction of the recycling flux with increasing γ corresponds to an increase of the global particle confinement time τ_p from 8 to 20 ms. The absolute values are depending on our assumption concerning the fraction of neutrals entering the plasma as molecules and on the ratio between flux to the limiter and flux to the wall. It is typical for the RI-mode that the external gas feed is closed almost completely and the discharge is only fueled by the neutral beam injection.

Spectroscopic investigations at a carbon test limiter positioned at the LCFS showed an increase of both the penetration depth of neutrals and the fraction of ionizations inside the LCFS with increasing γ [21]. These variations tend to steepen the density profile due to a shift of the total ion source distribution to smaller radii. This effect can be understood using a very simple model (cf. e.g. [18]). Assuming pure diffusive transport with a diffusion coefficient D and a δ-like particle source at $r = a - \lambda_{i0}$, the ratio between the plasma density in the center $n(0)$ and the density at the LCFS $n(a)$ can be described with the density decay length in the SOL $\lambda_n (n(a) \ll n(0))$ as

$$\frac{n(0)}{n(a)} = \frac{\lambda_{i0}}{\lambda_n}. \quad (1)$$

An additional inward pinch velocity v characterized by a shaping factor $S = -(v/D)(a^2/r)$ will lead to a further increase of $n(0)$ by a factor $\exp(S/2)$. Ionization in the SOL will affect the ratio between central and edge density through its effect on $\lambda_n (\lambda_n \sim 1/\sqrt{f}$, where f is the fueling efficiency and $(1 - f)$ the fraction of ionizations occurring in the SOL [18]).

From the changes of λ_{i0} and λ_n observed experimentally we expect an increase of $n(0)/n(a)$ by a factor 1.5 going from $\gamma = 35\%$ to $\gamma = 85\%$. Measurements of the density profile show an increase by a factor of 2, indicating an additional change of the shaping factor S, which amplifies the effect of the ion source distribution on the density profile significantly. The increase of the anomalous inward drift in discharges with radiation cooling has been attributed to the reduction of the edge temperature connected with a steepening of the temperature profile and a subsequent steepening of the density profile due to relaxation to "canonical" profiles with $n_e(0)/n_e(a) = (T_e(0)/T_e(a))^{1/2}$ (cf. discussion in [23]).

The improvement of energy confinement in the RI-mode is clearly correlated with the peaking of the density profiles. Peaked density profiles have a stabilizing effect for several instabilities driving anomalous transport like ITG-modes and ETG-modes (cf. [24]). Such a reduction of heat transport could be seen modeling the transport of impurities and their effect on particle and heat transport in a self-consistent way using the RITM-code [25]. It is observed experimentally that – for a given plasma current and heating scenario – a certain threshold of the density peaking factor defined by $\bar{n}_{e0}/\langle n_e \rangle$ must be overcome to obtain the transition to improved confinement. Fig. 6 illustrates these findings, showing the enhancement factor f_{H93} versus the ratio between the line averaged central electron density $\bar{n}_{e0}$ and the volume averaged electron density $\langle n_e \rangle$ starting 200 ms before the injection of neon up to 500 ms after the beginning of the feedback controlled neon seeding for a typical RI-mode discharge (solid line). Three different phases can be distinguished: (1) an increase of the peaking factor without substantial increase of the energy confinement (the first 40 ms after the start of the neon seeding, (2) the transition to improved confinement with a steep increase of f_{H93} for $\bar{n}_{e0}/\langle n_e \rangle \approx$ 1.2 and 3) a slight additional increase of density peak-

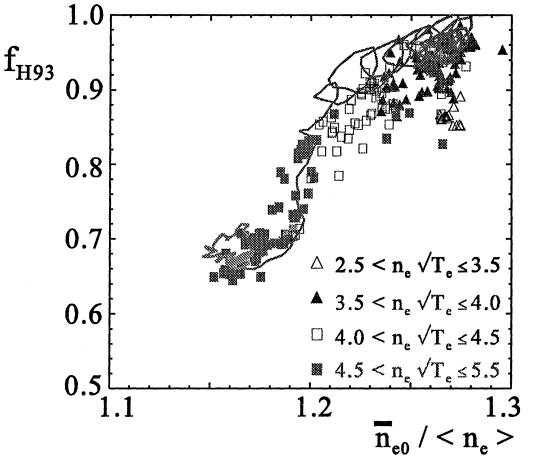

Fig. 6. Enhancement factor f_{H93} of the energy confinement time with respect to the ELM-free H-mode scaling against the ratio between line averaged central and volume averaged electron density for a typical RI-mode discharge (solid line) and the data set shown in Fig. 3 ($\bar{n}_{e0} = 0.8$–$1.1 \times n_{GW}$, $P_{heat} =$ 2.0–3.0 MW, $I_p = 400$ kA, different symbols indicate different values of the product $n_e\sqrt{T_e}/10^{19}$ m$^{-3}\sqrt{\text{eV}}$).

ing when the confinement has reached its highest value ($f_{H93} \approx 1$). In addition the relation between f_{H93} and $\bar{n}_{e0}/\langle n_e \rangle$ is displayed for all the time slices shown in our edge operational diagram (Fig. 3). Different symbols indicate different intervals of the product $n_e \sqrt{T_e}$ as a measure of the penetration depth at the edge. All the discharges follow the trend shown for the trajectory of our RI-mode example (solid line). The resulting global peaking factor $\bar{n}_{e0}/\langle n_e \rangle$ is clearly correlated with our measure of the penetration depth.

Fueling by *strong gas puffing* during the RI-mode phase has been found to lower the energy confinement time substantially. We find an increased density decay length in the SOL, higher edge density and a smaller penetration depth of neutrals in discharges with strong gas puffing. The density profile is less peaked compared to RI-mode discharges without gas fueling at the same γ. *Pellet injection* on the contrary, can provide deep fueling. It has been found that the density during the RI-mode can be increased without losing the good energy confinement by injecting pellets in TEXTOR-94 [26].

The *horizontal position of the plasma* has been found to be a critical parameter for optimal confinement. Shifting the plasma to the high field side onto the inner bumper limiter generally inhibits the transition to the RI-mode in spite of high radiation levels as the gas consumption is increased when the plasma is positioned at the high field side due to increased wall pumping [27].

Such a strong relation between edge conditions and global confinement properties as observed in the RI-mode has also been found for Improved Ohmic Confinement (IOC) as discussed e.g. in Ref. [28]. In this paper we concentrated on the influence of recycling and fueling properties on the density profile, but the increase of the shear of toroidal plasma rotation in the RI-mode observed with unbalanced neutral beam heating [21] may also contribute to the improvement under such experimental conditions due to the stabilizing effect of $E \times B$ shear (cf. [25]).

5. Impurity production in the RI-mode

The substantial reduction of deuterium flux due to the improved particle confinement in discharges with a radiating boundary strongly affects the impurity production at the main limiter ALT II. The absolute fluxes of carbon and oxygen, the most important *intrinsic* impurities, are reduced with increasing γ. However, the reduction is not as high as for deuterium, so that the effective yields (relation between impurity and deuterium fluxes) increase. Fig. 7 displays the ratios Γ_{Ne}/Γ_D (in the SOL at $R - R_0 = 49$ cm), Γ_C/Γ_D and Γ_O/Γ_D (measured spectroscopically at the ALT-II limiter) as a function of γ for two series of discharges at $\bar{n}_{e0} = 5.0 \times 10^{19}$ m^{-3} ($0.85 \times n_{GW}$) and $\bar{n}_{e0} = 6.0 \times 10^{19}$m^{-3} ($1.0 \times n_{GW}$). The increase of the yields of carbon and oxygen is less marked at the higher density. The flux ratio between neon and deuterium needed to establish a radiating boundary where 80% of the total input power is radiated and reaches values up to 0.08 for the lower and up to 0.05 for the higher density.

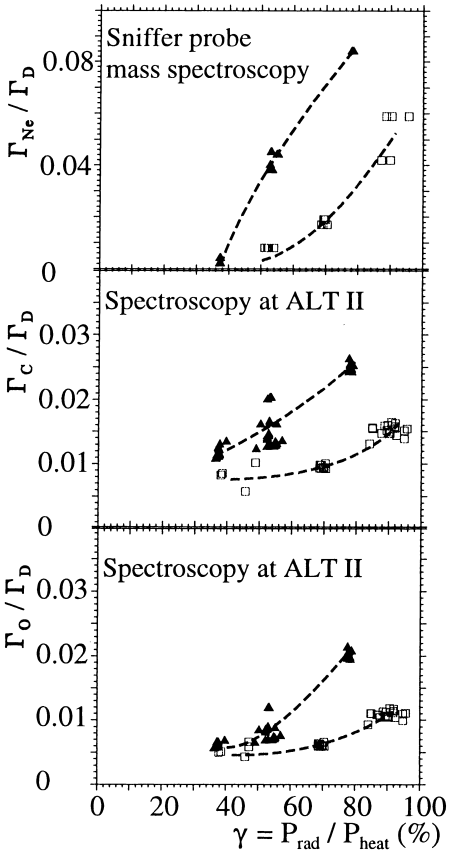

Fig. 7. Flux rations of impurities determined by mass spectroscopy in the SOL or with optical spectroscopy at the ALT-II limiter against radiation level γ ($\bar{n}_{e0} = 0.85 \times n_{GW}$ (full triangles), $\bar{n}_{e0} = 1.0 \times n_{GW}$ (open boxes), $P_{heat} = 2.0$–3.0 MW, $I_p = 400$ kA).

Using the experimentally determined flux ratios of neon and oxygen and the electron temperature at the LCFS we calculate the variation of total sputtering yield of carbon when increasing radiation based on the Bohdansky equations [29] for the lower density of $\bar{n}_{e0} = 5 \times 10^{19}$ m^{-3}. We assume an average ionization stage of $\langle Z \rangle = 3$ for carbon, $\langle Z \rangle = 4$ for oxygen and $\langle Z \rangle = 5$ for neon. These values are derived from calculations made with the RITM-code and in agreement with measurements by ion mass spectrometry at TEXTOR [30]. Fig. 8 shows the variation of the different contributions to the total sputtering yield calculated according to

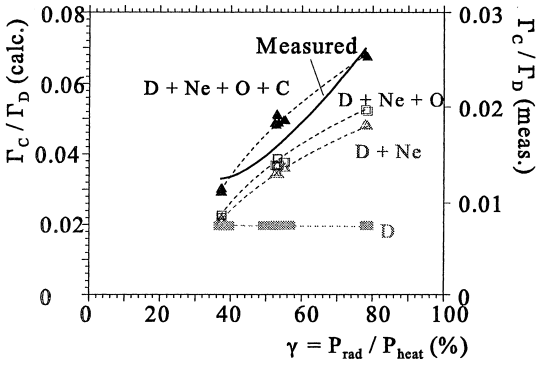

Fig. 8. Calculated sputtering yields of graphite bombarded with D^+, Ne^{5+}, O^{4+} and C^{3+} ($\bar{n}_{e0} = 0.85 \times n_{gw}$, $P_{heat} = 2.2$–2.7 MW, $I_p = 400$ kA) in comparison with measured yield against radiation level γ.

$$\frac{\Gamma_C}{\Gamma_D} = \frac{Y_D^C + \frac{\Gamma_{Ne}}{\Gamma_D} Y_{Ne}^C + \frac{\Gamma_O}{\Gamma_D} Y_O^C}{1 - Y_C^C}, \quad (2)$$

where Y_D^C, Y_{Ne}^C, Y_O^C and Y_C^C denote the sputtering yields for deuterium, neon and oxygen on graphite and the carbon self-sputtering yield for impact energies of the sputtering ions calculated with the charge states mentioned above and assuming $T_e = T_i$. The yield for carbon sputtering due to deuterium is about constant at 2%. Sputtering by neon is a major contribution to the total yield due to the high flux ratios necessary to establish the high radiation. As a consequence the carbon yield increases with γ in spite of the reduction of the edge temperature. This trend is also seen in the measurements. However, the measured absolute yields are roughly a factor 2.5 smaller than the calculated ones. This could be partly attributed to the uncertainty within the absolute determination of the deuterium flux due to the molecular contribution. In addition, one could speculate about a possible deviation of the neon flux ratio at the limiter tip with respect to the ratio measured in the SOL by the sniffer probe. In any case, we conclude, that a higher plasma density is much more favorable concerning the release of carbon in the RI-mode because the neon flux with respect to the deuterium flux is lower.

Concerning the production of oxygen another process becomes important with increasing radiated power: *photon induced release of impurities adsorbed at the walls*. Fig. 9 gives an indication for this process showing the neutral gas pressure of CO, CO_2 and of the hydrogen molecules measured at the wall as a function of γ. The hydrogen pressure decreases with increasing γ similar to the flux at the limiter. Opposite to that the CO pressure remains constant and the CO_2 pressure is even increasing. This demonstrates that the release of CO_2 and of a part of CO is not coupled to the deuterium flux to the walls but is due to photon impact which increases uniformly. The importance of this process has been shown earlier in TEXTOR [31]. Photons reaching the wall can produce free electrons in the surface which then enable the release of CO and CO_2 molecules attached to the wall as ions by charge transfer. This release mechanism may partly explain the increase of the flux ratio Γ_O/Γ_D with γ.

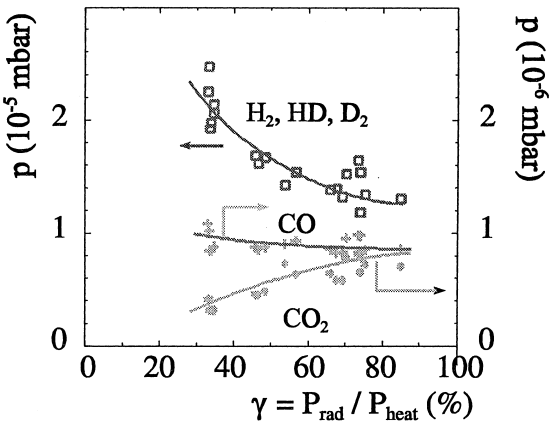

Fig. 9. Neutral pressures of deuterium and hydrogen molecules, CO and CO_2 against radiation level γ ($\bar{n}_{e0} = 0.85 \times n_{GW}$, $P_{heat} = 2.2$–2.7 MW, $I_p = 400$ kA).

The substantial amount of neon and the increase of the effective yields of the intrinsic carbon and oxygen lead to an increased dilution at the plasma boundary. This is evident if we compare the reduction of the deuterium flux recycling at the ALT-II limiter with the reduction of the product $n_e \sqrt{T_e}$ which is a measure of the deuterium flux to the limiter *disregarding* any dilution (cf. Fig. 10). To estimate the deuterium concentration at the plasma boundary we use the flux ratios Γ_i/Γ_D

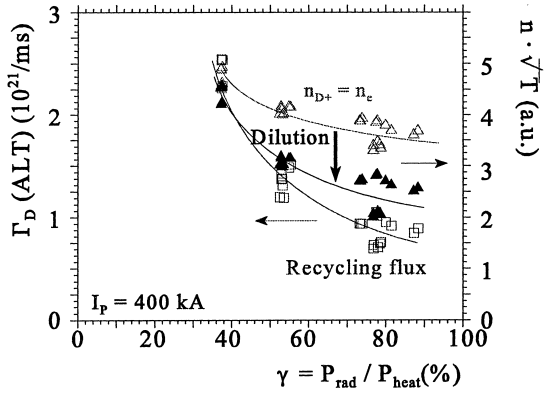

Fig. 10. Deuterium flux to the limiter calculated from n_e and T_e at the LCFS in comparison with flux measured by spectroscopy against radiation level γ ($\bar{n}_{e0} = 0.85 \times n_{GW}, P_{heat} = 2.2$–$2.7$ MW).

between impurity and deuterium neutrals ($i = \mathrm{Ne}, \mathrm{C}, \mathrm{O}$) shown in Fig. 7. The flux ratio $\Gamma_i/\Gamma_\mathrm{D}$ is related to the ionic concentration of an impurity species i, n_i/n_D, by $\Gamma_i/\Gamma_\mathrm{D} = (v_i\ n_i)/(c_\mathrm{s}\ n_\mathrm{D})$ where v_i denotes the velocity of impurity ions entering the Debye sheath in front of the limiter surface and c_s the ion sound velocity of deuterium. Due to friction forces between impurity and deuterium ions the ion velocity v_i approaches c_s at high densities and low temperatures in the SOL [32]. Therefore, we assume $\Gamma_i/\Gamma_\mathrm{D} = n_\mathrm{i}/n_\mathrm{D}$ to estimate the dilution at the edge. In fact, Γ_i / Γ_D gives a *lower* limit for the ionic impurity concentration at the plasma edge as $v_i \leqslant c_\mathrm{s}$. Using the condition of quasi-neutrality, $n_\mathrm{e} = n_\mathrm{D} + \Sigma\langle Z\rangle_i n_i$ where all impurity species i have to be added up and $\langle Z\rangle_i$ denotes their average charge state, the deuterium concentration n_D / n_e can be expressed as

$$\frac{n_\mathrm{D}}{n_\mathrm{e}} = \left(1 + \sum_i \langle Z\rangle_i \frac{\Gamma_i}{\Gamma_\mathrm{D}}\right)^{-1}. \tag{3}$$

Using this formula to correct the deuterium flux to the limiter we find reasonable agreement between the reduction of the deuterium flux measured spectroscopically and the deuterium ion flux to the limiter calculated (Fig. 10).

The deuterium concentration at the edge according to (Eq. (3)) is reduced from 0.9 at $\gamma = 35\%$ down to less than 0.7 at $\gamma = 85\%$. However, there are remarkable differences concerning the dilution in the plasma center compared to the dilution at the edge. The central deuterium concentration $c_\mathrm{D}(0)$ is calculated with the help of the carbon and neon concentration measured by CXRS on axes. The ratio between carbon and oxygen density in the center has been assumed to be equal to the ratio of carbon and oxygen flux at the ALT-limiter. Neon, carbon and oxygen are assumed to be fully ionized. Using the condition for quasi-neutrality we obtain a central deuterium concentration $c_\mathrm{D}(0)$ only slightly decreasing from 0.86 at $\gamma = 35\%$ to 0.81 at $\gamma = 85\%$. This almost constant dilution can be understood by the partial replacement of carbon in the center (with central concentrations decreasing from 0.014 at $\gamma = 35\%$ to 0.01 at $\gamma = 85\%$) by neon with a concentration of 0.009 at $\gamma = 85\%$. These findings are consistent with an analysis of the neutron reactivity measured in the plasma [33]. The effective charge of the plasma, Z_eff in the center is calculated with the help of the impurity concentrations from the CXRS measurements and increases from 1.8 to 2.5 with increasing γ despite the constant dilution as carbon is replaced by neon with a higher charge number Z. The comparison of the deuterium concentration at the edge and in the plasma center and its variation with increasing γ indicates a hollow distribution of the impurity concentration over the plasma radius, able to provide a strongly radiating plasma boundary whereas the plasma reactivity in the center is only weakly affected.

6. Summary and conclusions

On the limiter tokamak TEXTOR-94 a regime combining power exhaust by a radiating plasma boundary with improved energy confinement at high plasma densities has been found, the *RI-mode*. We have described the substantial changes of plasma edge properties which can be observed when the radiating boundary is formed: the edge temperature and density are reduced and the particle transport out of the confined volume decreases characterized by a reduction of the particle diffusion coefficient at the LCFS. In an edge operational diagram relating temperature and density at the LCFS the discharges with improved confinement are clearly separated from those with L-mode confinement. The product $n_\mathrm{e}(a)\sqrt{T_\mathrm{e}}(a)$ turns out to be a suited parameter to distinguish RI-from L-mode in terms of edge parameters. It represents a rough measure of the ionization rate of neutrals and determines their penetration depth the confined volume. This finding indicates, that the increase of the penetration depth and of the fueling efficiency, which has been experimentally proven by spectroscopic measurements of the ion source distribution near a test limiter, are important parameters for the RI-mode. This extension of the radial ion source distribution towards smaller radii adds to the steepening of the density profile due to an increased inward drift observed in the RI-mode. For a given heating scenario the transition to improved confinement occurs as soon as a critical threshold with respect to the peaking of the density profile is reached. If the favorable changes at the plasma edge towards deeper penetration and steeper density profiles are suppressed, e.g. by strong gas puffing, the transition to improved confinement is generally inhibited.

The reduction of the deuterium flux at the main limiter leads to a reduction of the fluxes of the intrinsic impurities carbon and oxygen. However, the effective yield of carbon with respect to deuterium is increasing due to increased sputtering by the seeded neon. The oxygen yield is increasing due to an enhanced photon induced release of carbon oxides from the wall. The injection of neon and the release of intrinsic impurities lead to a substantial dilution at the plasma edge. The plasma center, however, is much less affected in the RI-mode, indicating different transport of deuterium with strongly peaked density profiles compared to neon and the intrinsic impurities which seem to have a much flatter radial distribution. Operation at the highest densities is favorable with respect to the release of impurities at the edge as well as with respect to the resulting impurity content in the plasma bulk.

In future, the analysis of the edge operational diagram for discharges in the RI-mode has to be extended to a broader range of global parameters like plasma current and magnetic field and to different heating scenarios.

Further understanding of the physical mechanisms behind the link between plasma edge and global confinement properties described in such a diagram will then help to investigate this regime on other machines and to assess its potential for the application in future devices.

Acknowledgements

The TEXTOR-94 team is gratefully acknowledged for providing excellent experimental conditions. We wish to thank H.R. Koslowski, J. Rapp and A. Krämer-Flecken for providing valuable experimental data and M. Tokar for clarifying discussions.

References

[1] U. Samm et al., Plasma Phys. Controlled Fusion 35 B (1993) 167.
[2] U. Samm et al., J. Nucl. Mater. 220–222 (1995) 25.
[3] M. Greenwald et al., Nucl. Fusion 28 (1988) 2199.
[4] A.M. Messiaen et al., Nucl. Fusion 34 (1994) 825.
[5] A.M. Messiaen et al., Phys. Rev. Lett. 77 (1996) 2487.
[6] A.M. Messiaen et al., Phys. Plasmas 4 (5) (1997) 1690.
[7] A.M. Messiaen et al., Comments Plasma Phys. Controlled Fusion 18 (4) (1997) 221.
[8] A. Kallenbach et al., Nucl. Fusion 35 (1995) 1231.
[9] J. Neuhauser et al., Plasma Phys. Controlled Fusion 37 A (1995) 37.
[10] G.M. Staebler et al., Proceedings of the 24th European conference on controlled fusion and plasma physics, Berchtesgaden, vol. 21 A, Part III, European Physical Society, 1997, p. 1093.
[11] G. Jackson et al., these Proceedings.
[12] J.V. Seggern, J. Nucl. Mater. 220–222 (1995) 677.
[13] A. Pospieszczyk, Diagnostic of edge plasmas by optical methods, in: R.K. Janev, H.W. Darwin (Eds.), Atomic and Plasma-material Processes in Controlled Thermonuclear Fusion, Elsevier, Amsterdam, 1993, p. 213.
[14] A. Pospieszczyk et al., these Proceedings.
[15] V. Philipps, E. Vietzke, M. Erdwig, J. Nucl. Mater. 162–164 (1989) 550.
[16] B. Schweer, M. Brix, M. Lehnen, these Proceedings.
[17] ITER H-Mode Database Working Group, Nucl. Fusion 34 (1994) 131.
[18] P.C. Stangeby, G.M. Mc Cracken, Nucl. Fusion 30 (1990) 1225.
[19] H. Zohm, Plasma Phys. Controlled Fusion 38 (1996) 1213.
[20] W. Suttrop et al., Plasma Phys. Controlled Fusion 39 (1997) 2051.
[21] B. Unterberg et al., Plasma Phys. Controlled Fusion 39 B (1997) 189.
[22] D.S. Gray et al., Nucl. Fusion, 38 (1998) 1585, also report UCSD-ENG-039.
[23] M. Tokar, R. Jaspers, B. Unterberg, Contrib. Plasma Phys. 38 (1998) 67.
[24] G.M. Staebler, Plasma Phys. Controlled Fusion 40 (1998) 581.
[25] M. Tokar, R. Jaspers, B. Unterberg, Nucl. Fusion 38 (1998) 961.
[26] J. Hobirk et al., Proceedings of the 24th European conference on controlled fusion and plasma physics, Berchtesgaden, vol. 21 A, Part IV, European Physical Society, 1997, p. 1861.
[27] J. Winter, J. Vac. Sci. Technol. A 5 (1987) 2286.
[28] K. Mc Cormick et al., J. Nucl. Mater. 176&177 (1990) 89.
[29] J. Bohdansky, Nucl. Instrum. Methods B 2 (1984) 587.
[30] G.F. Matthews et al., J. Nucl. Mater. 196–198 (1992) 253.
[31] V. Philipps, E. Vietzke, M. Erdweg, J. Winter, J. Nucl. Mater. 200 (1993) 355.
[32] M. Tokar, Contrib. Plasma Phys. 34 (2/3) (1994) 344.
[33] G. Van Wassenhove et al., Proceedings of the 24th European conference on controlled fusion and plasma physics, Berchtesgaden, vol. 21 A, Part IV, European Physical Society, 1997, p. 1679.